Error measurement accuracy methodology – Technical report - Metrological performances of self-calibrating X-ray computed tomography system with helical trajectory

Abstract:

New type of methods allows minimising the geometrical misalignments and they are called self-calibrating algorithms. This algorithm provides theoretically exact reconstruction when linked with the helical geometry, implying images without geometric distortion. CT systems applying such algorithms do not potentially need any additional calibration or even reference measurement. We propose a methodology of testing such a system with a self-calibrating algorithm and helical trajectory. Moreover, the length measurement error is evaluated on both spheres distance error and probing errors. Sphere distance errors are reaching 2/3 of the voxel size. Besides, we show the results for the length measurement error following the VDI/VDE 2630 guideline. The results show that the sphere distance errors has still a systematic error. This stems from the calibration being highly dependent on knowing the average voxel size with sufficient precision. The magnification is given by the self-calibration algorithm and it is associated with the detector pixel size. Therefore, the detector pixel size needs to be specified with precision down to 10 nm. This is below the manufacturing tolerance of the detector, and therefore it needs to be measured for each detector separately. In this paper, we provide a statistical method for obtaining this calibration. With this calibration, we achieve an SD error of $\pm (18.63 + 2.5L/100)$, when imaging with a voxel size of about 15µm. In addition to that, we introduce the procedure to evaluate the maximal permissible error calculation on pure statistics based on the length measurement error. Reconstruction Discussion is focused on the stability of reconstruction and the results of individual errors.

Theory:

The proposed work employs the algorithm called auto-focus presented in Kingston et al. [1] and Varslot et al. [2]. They proposed a method for compensation of geometrical misalignments, which uses acquired data itself for calibration without the usage of any other calibration artefacts or instruments.

Using the standard and several types of guidelines are one way of the CT measurement precision evaluation. Although, the researchers and CT developers are focusing on the error sources and its evaluation, currently, a German guideline VDI/VDE 2630 [3] part 1.3 is the only standard focusing on performance verification and acceptance testing of CT devices. The guideline uses reference objects and the evaluation of the reconstructed data. It uses two complementary types of tests which are similar for evaluation of CMM performance. Local P-test (probing error test) tests the performance of measurement significantly smaller than reconstructed volumes. Respective characteristics for P-test are probing error of form and probing error of size. Another important characteristic is the global E-test. It evaluates measurements in the entire measured volume; the corresponding characteristics are sphere distance errors. The global error is called length measurement error (E) and it is the result of both sphere distance error and probing error. Carmignato et al. [4] show that scientists design reference objects following the requirements of the individual CT system to set its metrological performance with the requirements set by [3].

Standard evaluation of measurement errors following VDI/VDE 2630 guideline:

Method A suggested by VDI/VDE guideline take sphere distance errors together with probing errors into account and determine the global error, as a length measurement errors (E) [3]. The Length measurement error is obtained as sphere distance error plus signed probing error of size and probing error of form. The calculation can be then described by the formula [3]:

$$E = L_{ka} - L_{kr} + P_S + \big(\mathrm{sgn}(L_{ka} - L_{kr} + P_S)\big)P_F. \qquad (1)$$

where L_{ka} is measured sphere distance, L_{kr} is calibrated sphere distance, P_s is probing error of size and P_f is probing error of form.

In this work, we selected unidirectional method A. The sphere distance error S_D and probing errors P_S and P_F are described in [4]. S_D defines the difference between the displayed value of test length (distance between centres of two balls) L_{ka} and calibrated length L_{kr}:

$$S_D = L_{ka} - L_{kr}. \qquad (2)$$

Measurement distances between the centres of two spheres are the unidirectional measurement. It means that it is much less affected by some of the different error sources such as threshold determination and therefore, can give information about geometry influence factors (misalignments of system components, scale determination).

Probing error of form is determined using a single sphere with calibrated diameter. Probing error of form (P_F) is defined as the difference between the maximum (R_{max}) and minimum (R_{min}) distances from the probing points to the centre of the regression sphere:

$$P_{\mathrm{Form}} = R_{max} - R_{min}. \qquad (3)$$

Probing error of size is defined as the difference between the measured diameter D_a and the calibrated diameter D_c of the sphere:

$$P_{\mathrm{Size}} = D_a - D_c. \qquad (4)$$

Proposed Maximum Permissible error characterization:

To our best knowledge, there is no setup standard presenting an approach of MPE calculation that would be widely accepted and used by the manufacturers. Our presented approach uses the standard way of calculating SEM (Standard Error of the Mean) and extends it in a way, so it could be used to calculate the MPE

In the first step, S_d is calculated according to (2). From all measured deviations at every distance, the maxima of absolute values are calculated. In the next step, an ordinary linear regression of the measured points is done. A general formulation is $y = a \cdot x + b$. In this model, a non-zero slope a indicate a magnification error, while the intercept b represents the errors coming from all other processes.

Secondly, our approach is based on the maximal values that will ensure the MPE will have sufficient range. The SEM of maximal values is calculated as:

$$\sigma = \sqrt{\frac{1}{n(n-1)}\sum_{i=1}^{n}(x_i - \bar{x})^2}, \qquad (5)$$

where n is the number of measurements and $\bar{x}$ is the arithmetic mean calculated from the maxima of absolute values of deviations. From this an expanded uncertainty $\bar{\sigma}$ is calculated as: $\bar{\sigma} = t \cdot \sigma$, where t is the coefficient related to the Student's t-distribution corresponding to an ensemble with

$n - 2$ degrees of freedom and the significance level $\alpha = 0.01$. Then the true value of mean should lie within the 99.9% confidence band prescribed by $\text{MPU} = \bar{x} \pm \bar{\sigma}$.

We get, that when accounting for the uncertainty of the complete measurement system, MPU should be less than 1/3 of the MPE for the actual conformity assessment. So, the MPE is calculated by equation (6).

$$MPE = 3 \cdot t \cdot SEM = 3 \cdot t \cdot \sqrt{\frac{1}{n(n-1)} \sum_{i=1}^{n} (x_i - \bar{x})^2},$$

where *t* is the student's coefficient which corresponds to the degree of freedom.

As the last step, we did an ordinary linear regression of the points received from MPE calculation, while taking into account the result of the previous linear regression of calculated errors. The regression line is then prescribed by $y = a \cdot x + b + \text{MPE}$, with *a* and *b* being the regression coefficients from the previous calculation. The whole line is then mirrored across the *x*-axis to reflect the negative values of measurement errors. The calibration standard is then prescribed by the regression coefficients: namely by slope ''*a*'' and new interception ''*b*'' + MPE.

Reference objects:

The purpose of our developed multi-ball phantom is to allow multiple length measurements in one CT scan. Our design allows us to measure several lengths in more than 4 spatial directions in one CT scan. To further reduce the influence of CT artefacts and measurement time, no more than two spheres overlap in the horizontal direction while acquiring the projection and so the exposure time is reduced. The multi-ball phantom consists of 13 ruby spheres of nominal diameter 4 mm. Ruby balls are glued on a polycarbonate plate 40 × 55 mm (Fig. 1). Advantage of the polycarbonate is its transparency for visible light which allow performing calibration using a coordinate measuring machine with an optical sensor. Also, we choose the polycarbonate plate due to its thermal stability (linear thermal expansion coefficient 65-70 10^{-6} /K).

The multi-ball phantom was scanned in three different positions two times in each (Fig. 1). The three positions were chosen concerning the [3] and perform the sphere error calculation in all directions needed to evaluate the maximal error of the system. The sample object and sample detector distances were chosen as standard positions of the sample and detector in HeliScan analysis of material science samples.
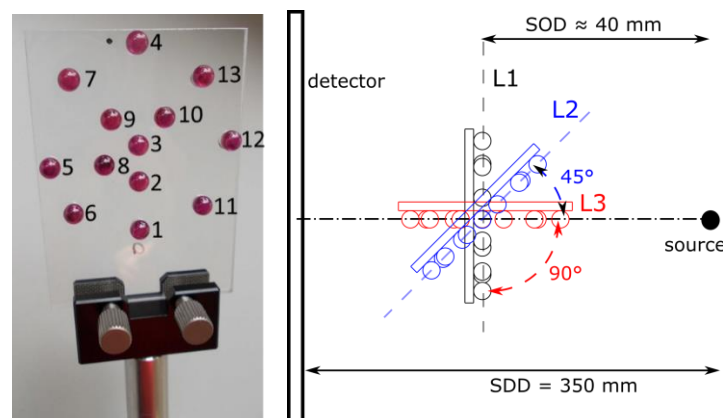

Figure 1: Plate with balls of nominal diameter 4 mm positioned according to the VDI/VDE guideline. The ball's positions allow 5 directions measurement in one scan. Multi-ball phantom positions chosen

according to [3]. L1, L2, and L3 are three different positions, always 45° rotated. The SOD is the source to object distance. The SDD is the source to detector distance. The scheme corresponds to the top view.

Ceramic ball of nominal diameter 10 mm and sample holder with 50 mm long carbon bar for off-centred scan for probing error (Fig. 2). The difference between the centre to the off-centre position is 13 mm. The position of the ceramic ball needs to be placed in the six different positions to examine the error approximately in the same volume as in the length error measurements. The sample holder allows off-centre scanning.

The reference [3] refers to the measurement of the probing error of form and size. The ceramic ball was used to perform and calculate probing errors. The plan for the ceramic ball positions was that all measurement can fulfil the reconstructed volume of the multi-ball phantom (Fig. 2).
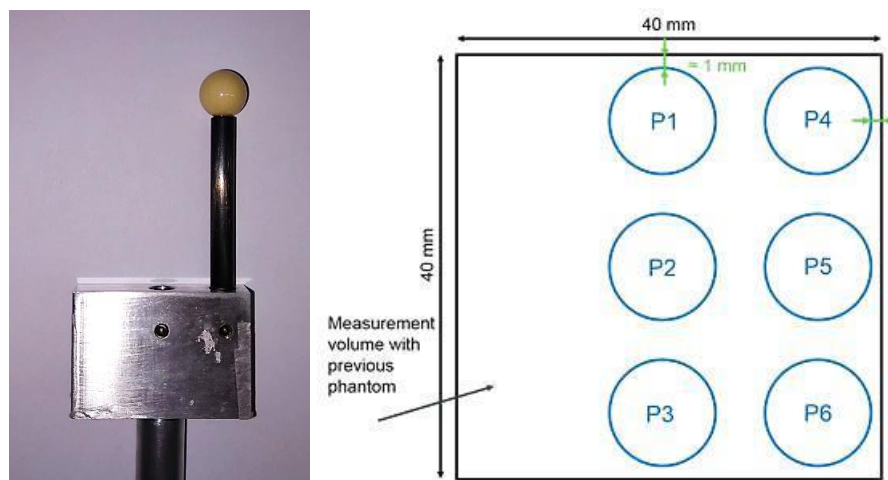

Figure 2: The sample holder allows the measurement of the ceramic ball in all of the six positions needed according to [3]. The box allows an in- and off-axis scan. Ceramic ball phantom positions according to were designed to fulfil the reconstructed volume of the multi-ball phantom. P1 to P6 is the labelling of the ceramic ball positions. The scheme corresponds to the front view of the reconstructed data.

Evaluation:

The scans were performed with an X-ray micrococcus tube with a tungsten target and wide cone angle ~ 160°. The high contrast detector 3072 × 3072 px with 139 μm pixel size. The exposure time was 0.7 s with five averaging in each of the 5954 positions with 2880 projections per evolution. In all measurements, the utilized acceleration voltage and X-ray currents were 100 kV and 160 μA, respectively. The beam was filtered with 0.22 mm of stainless steel. The detector position together with the sample stage was placed in the current position newly each scan.

Last but not least, we used proposed statistical method for the calculation of MPE. The MPE of the not calibrated system was stated as **± (10.07+ 15.6L/100)**. This was achieved using scans with voxel size of about 15μm. This accuracy will clearly depend on the largest distance in the scan between which there are features with the self-calibration algorithm can use to determine image quality. The algorithm is therefore best suited for imaging samples with lots of structure, such as foams, rock samples, and intricate structures.
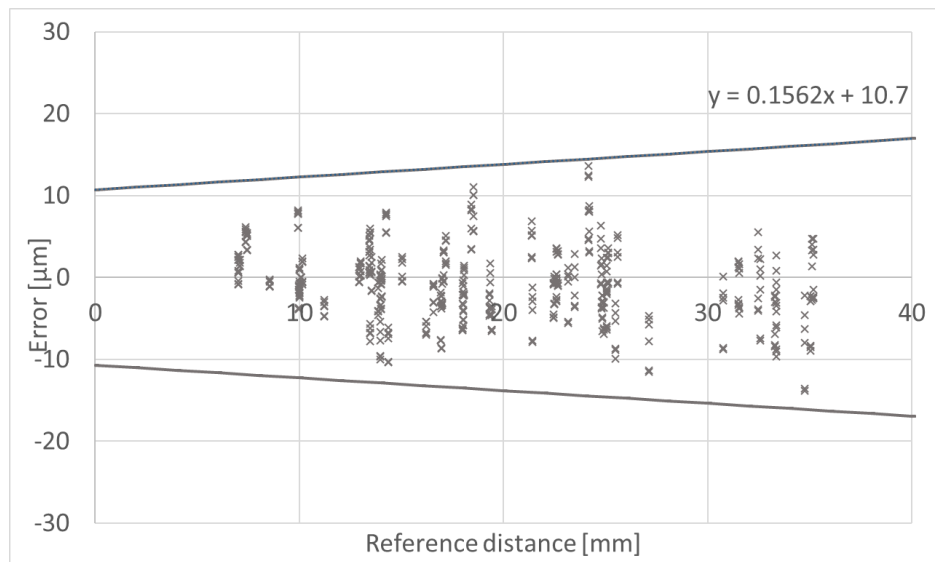
Figure 7: Sphere distances measurement errors were divided into groups according to their direction in reconstructed volumes.

To enhance the statistical importance of our results, there is a need for a bigger number of measurements to be evaluated. Still, the slope 0.025 is describing the error in the magnitude and so the voxel size determination to be less than 0.04 %. This is equivalent to 1 voxel distance error across the horizontal field of view

Literature:

[1]   A. M. Kingston, G. R. Myers, S. J. Latham, B. Recur, H. Li, A. P. Sheppard. Space-Filling X-Ray Source Trajectories for Efficient Scanning in Large-Angle Cone-Beam Computed Tomography. IEEE Transactions on Computational Imaging [online]. 2018, 4(3), 447-458. DOI: 10.1109/TCI.2018.2841202. ISSN 2333-9403. Available: https://ieeexplore.ieee.org/document/8367874/

[2]   T. Varslot, A. Kngston, G. Myers, A. Sheppard. High-resolution helical cone-beam micro-CT with theoretically-exact reconstruction from experimental data. Medical Physics [online]. 2011, 38(10), 5459-5476 [cit. 2019-11-13]. DOI: 10.1118/1.3633900. ISSN 00942405. Dostupné z: http://doi.wiley.com/10.1118/1.3633900

[3]   VDI/VDE 2630-1.3: 2011–12 (2011) Computed tomography in dimensional measurement—guideline for the application of DIN EN ISO 10360 for coordinate measuring machines with CT-sensors

[4]   S. Carmignato, W. Dewulf, R. Leach, Industrial X-ray computed tomography, Springer International Publishing, Cham, 2017. https://doi.org/10.1007/978-3-319-59573-3.